Available online at www.sciencedirect.com
ScienceDirect
Composite Structures 79 (2007) 288–299
COMPOSITE STRUCTURES
www.elsevier.com/locate/compstruct

Experimental validation of vibration-based damage detection for static laminated composite shells partially filled with fluid

L. Yu [a,b], L. Cheng [a,*], L.H. Yam [a], Y.J. Yan [b], J.S. Jiang [b]

[a] Department of Mechanical Engineering, The Hong Kong Polytechnic University, Hung Hom, Kowloon, Hong Kong SAR, China
[b] Institute of Vibration Engineering, Northwestern Polytechnical University, Xi'an, 710072, China

Available online 25 January 2007

Abstract

A vibration-based damage detection method for a static laminated composite shell partially filled with fluid (LCSFF) is presented and validated by experiment. The crack damage is simulated using advanced composite damage mechanics in a dynamic finite element model, in which the interaction between the fluid and the composite shell is considered. The accuracy of FE model is first validated by comparing the computed and measured structural frequency response function. Structural damage indexes are constructed and calculated based on energy variation of the structural vibration responses decomposed using wavelet package before and after the occurrence of structural damage. An artificial neural network (ANN) is trained using numerically simulated structural damage index to establish the mapping relationship between the structural damage index and damage status. The test specimen used in experiment contains a cut in its surface made by laser cutting system. Response signals of both intact and damaged specimen are measured and used to construct the corresponding damage indices. The damage status is successfully identified using ANN, indicating that the method adopted in this paper can be applied to online structural damage detection and health monitoring for static LCSFF.

Keywords: Composite shell; Fluid; Damage detection

1. Introduction

Shell structures made of composite materials have been extensively used in industry and engineering, e.g. aerospace, civil engineering, marine, petrochemical engineering and nuclear power generation due to their high strength-to-weight ratio, better corrosion resistance as well as the advantages of composite materials. However, many factors, such as aging, impact and fatigue will inevitably cause damages in composite material structures. Damages in the laminated composite shells partially filled with fluid will cause serious fluid leakage problems, and lead to catastrophe and economic loss. Damage detection systems for the LCSFF are therefore crucial to the safety and cost-effective operation of various composite pipelines and vessels.

Online damage detection is needed for some special devices, such as airplanes and spacecraft during flight, chemical engineering facilities located in poisonous or harmful environments, or underground pipelines, which cannot be easily accessed. Existing damage detection systems, such as X-ray and ultrasonic scan, cannot meet the requirement of online damage detection for such situations, since manual installation and inspection are usually required, and the actuators and sensors are sometimes bulky.

Dynamic damage detection methods have the potential to meet such requirements. There methods are based on the fact that damages in a structure result in a change in structural dynamic characteristics. Early investigations about dynamic damage detection method were conducted by Schultz and Warwick [1] (1971) and DiBennedetto et al. [2] (1972). Since then, research work in this field continued to flourish. Dynamic damage detection usually contains three basic steps: i.e., the measurement of structural

* Corresponding author. Tel.: +852 2766 6769; fax: +852 2365 4703.
E-mail address: mmlcheng@polyu.edu.hk (L. Cheng).

0263-8223/$ - see front matter © 2006 Elsevier Ltd. All rights reserved.
doi:10.1016/j.compstruct.2006.11.008

dynamic data, the construction of damage index from the data, and provision of information for structural damage status from damage index. In each step, various methods have been developed.

The main requirement on measurement equipment for damage detection is high sensitivity. Due to the limit of online implementation, small volume and light weight are also necessary. Piezoelectric patches have the advantage in sensitivity, weight and volume. Furthermore, they also have the capacity to function in either passive or active modes, to serve as both sensors and actuators. Therefore, many researchers use embedded and/or surface mounted piezoceramic patches to generate the excitation, and to measure the corresponding dynamic data [3,4]. Other methods, such as optical fibre, have also been adopted in some work [5].

For the early discovery of incipient damage and continuous monitoring of the growth and location of damage, an online damage detection system must be able to indicate small damage. However, small damage only produces a very small change in structural dynamic characteristics. Therefore, the damage indices with high sensitivity are required. Possible candidates, which have been explored in the past, are natural frequencies [6], frequency response function (FRF) [7,8], flexibility matrix [9], mode shapes [10] and structure dynamic responses [11,12]. Now, even when the ratio of damage size to the total structural size is as small as the order of 0.01–0.1%, the structural damage can still be detected using the energy spectrum variation obtained by wavelet analysis [12]. However, the variation of environmental conditions can also cause the change in structural dynamic characteristics. Therefore, it is important to study how to remove the effect caused by environmental conditions while still keeping in the advantage of the high sensitivity of the index to damage [13,14].

Deduction from structural damage index to practical damage status is mathematically an inverse problem which is difficult to acquire precise solution using mathematical analysis only. Therefore, the soft computing techniques, such as ANN [7,12,15,16] and genetic algorithm (GA) [10,17,18], have been used by many researchers to solve this inverse problem as an optimization problem owing to their excellent pattern recognition capability. Data required for training ANN or running GA are usually provided by numerical simulations based on established FE structural model.

Although great progress has been made in the past, most of the presented works only demonstrated their feasibility through numerical simulations. A few experimentally validated works are limited in beam-like [3] and plate [19,20] structures. To our knowledge, investigation on on-line damage detection for shells partially filled with fluid (SFF) can scarcely be found.

A shell structure is considered as a simple structure in FE modeling. Once filled with fluid, however, the interaction between the fluid and the shell significantly increases the degree of difficulty in FE modeling.

In this paper, a practical damage detection method for static SFF is investigated; and experimental validation is successfully carried out in a static laminated composite SFF (LCSFF). A dynamic FE model of static LCSFF is established using the fluid–structure interaction theory. The crack is simulated in the FE model using advanced composite damage mechanics and is machined in the test specimen using a laser-engraving system. The change in energy spectrum of the decomposed wavelet signals of structural dynamic responses is adopted as the damage index. An ANN is trained using the numerically simulated data. The accuracy of the FE model is firstly validated through the experimental measurement of FRF. Then the experimental damage identification is carried out. The damage status of the experimental specimen is successfully identified by the ANN, showing that the damage detection method adopted in this paper provides effective ways for online health monitoring of static LCSFF.

2. Finite element model of static LCSFF with damage

2.1. Fluid-structural interaction theory in finite element method

In this study, the fluid (water) contained in the static LCSFF is static without sloshing and mean flow. The mean density and pressure are uniform throughout the fluid. The fluid is also assumed to be compressible and inviscid without viscous dissipation.

Under these assumptions, the fluid momentum (Navier–Stokes) and continuity equations can be simplified to get the discretized wave equation as follows:

$$[M_f]\{\ddot{P}_e\} + [C_f]\{\dot{P}_e\} + [K_f]\{P_e\} + \rho_f[R_e]^T\{\ddot{u}\} = 0 \tag{1}$$

where $[M_f]$, $[C_f]$ and $[K_f]$ are the fluid mass, damping and stiffness matrices, respectively. P_e is the nodal pressure vector; ρ_f the mean fluid density; $\rho_f[R_e]$ the coupling mass matrix at the fluid–structure interface, and is given by

$$\rho_f[R_e] = \rho_f \int_s \{N'\}\{N\}^T\{n\}\,dS \tag{2}$$

where $\{N'\}$ is the element shape function for displacement components u, v, and w (obtained from the structural element); $\{n\}$ the normal at the fluid boundary; $\{N\}$ the element shape function for pressure; S the surface where the derivative of pressure normal to the surface is applied.

The equation of motion for a linear structure with the fluid loading acting at the interface is:

$$[M_s]\{\ddot{u}\} + [C_s]\{\dot{u}\} + [K_s]\{u\} = \{F^a\} + \{F_e^{pr}\} \tag{3}$$

in which $\{F_e^{pr}\}$ is the fluid loading vector exerted on the interface S, and can be obtained by integrating the pressure over the area of the surface:

$$\{F_e^{pr}\} = \int_S \{N'\}\{N\}^T\{n\}\,dS\{P_e\} = [R_e]\{P_e\} \tag{4}$$

Then, the fluid–structure interaction problem can be written in an assembled form as:

$$\begin{bmatrix} [M_s] & [0] \\ [M^{fs}] & [M_f] \end{bmatrix} \begin{Bmatrix} \{\ddot{u}\} \\ \{\ddot{P}_e\} \end{Bmatrix} + \begin{bmatrix} [C_s] & [0] \\ [0] & [C_f] \end{bmatrix} \begin{Bmatrix} \{\dot{u}\} \\ \{\dot{P}_e\} \end{Bmatrix} + \begin{bmatrix} [K_s] & [K^{fs}] \\ [0] & [K_f] \end{bmatrix} \begin{Bmatrix} \{u\} \\ \{P_e\} \end{Bmatrix} = \begin{Bmatrix} \{F^a\} \\ \{0\} \end{Bmatrix} \quad (5)$$

where $[M^{fs}] = \rho_f [R_e]^T$ and $[K^{fs}] = -[R_e]$.

2.2. Finite element realization

The FE model is established according to an LCSFF specimen, which will be later used for experimental study, having the following dimensions: mean radius $R = 36$ mm, wall thickness $t = 2$ mm, and length $L = 280$ mm. The shell is made of resin glass fibre with orthogonal layer $(-60^\circ/0^\circ/60^\circ)_{30}$, having the following material properties: $E_1 = 47.518$ GPa, $E_2 = 4.588$ GPa, $G_{12} = 2.10$ GPa, $\mu_{12} = 0.4495$, $\mu_{21} = 0.0434$, and $\rho = 1860$ kg/m^3.

Dimensions and the meshing of the LCSFF model are shown in Fig. 1. The FE model consists of 552 (23×24) eight-node shell elements with three degrees of freedom (DOF) at each node [21,22] in the part of the shell wall, and 108 shell elements of the same type for the bottom part. 1944 3-D fluid elements [23] are used for fluid, when the fluid level is 78.26% of the shell's height. Although different kinds of boundary conditions are allowed in this FE model, free boundary conditions are used for the sake of convenience in experiment.

2.3. Crack damage simulation in the FE model

Depicting the geometry of the damage directly seems to be a natural way for simulating damage in structural dynamics FE model. However, in addition to the requirement of excessive meshes and the subsequent time-consuming calculations due to the large number of meshes involved, different meshings required by different damage sizes will also cause significant numerical error. Such error may even cover the effect produced by small structural damages on structural dynamic characteristics, such as natural frequencies. Therefore, the direct mesh method is not suitable for simulating crack in damage detection [24]. In fact, local damage in a structure always causes a decrease in structural local stiffness, and these variations can be reflected by changes in local structural material elastic coefficients. Hence, damage in a structure can be simulated in the FE model by modifying the elastic moduli of the elements at damage location. In some work [16,25], all of the elastic moduli are supposed to have the same decease after damage, which seem to be appropriate in the theoretical studies. However, studies in micro-damage mechanics show that the percentage of reduction for different elastic

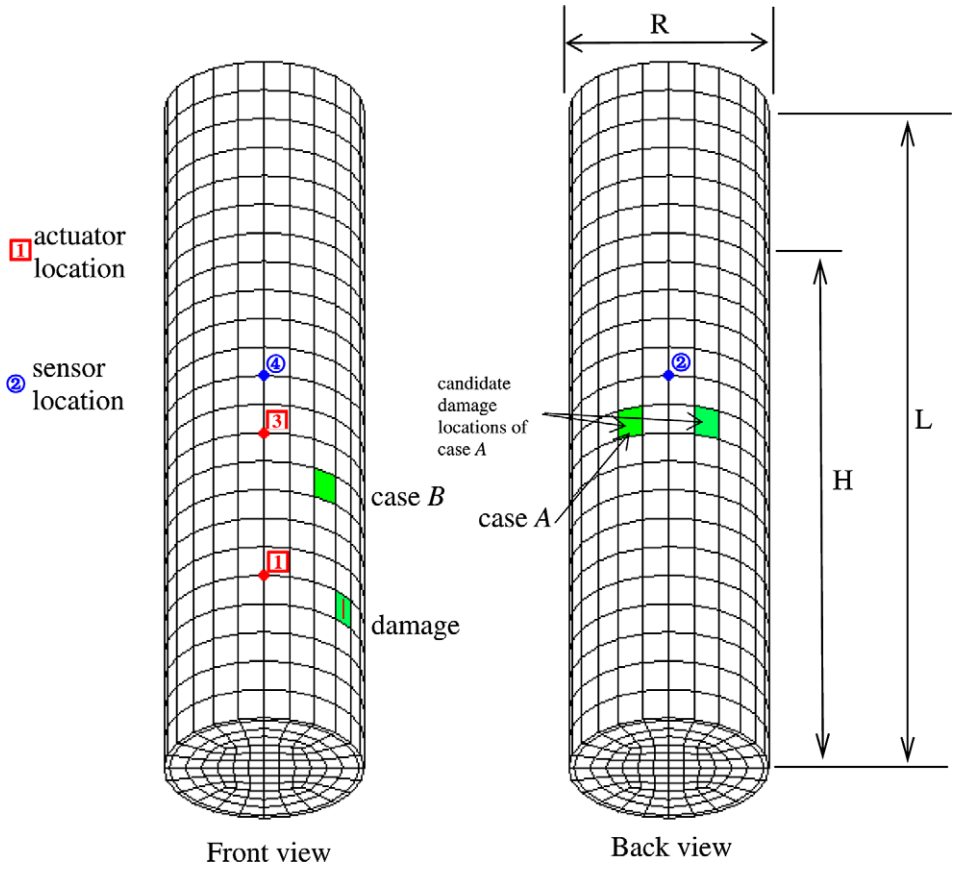

Fig. 1. Model of a composite shell partially filled with fluid.

moduli caused by damage is different [26]. Therefore, the following formulation for composite materials with crack damage proposed in ref [26] is adopted to calculate the variations of local elastic modulus in this paper.

$$\left.\begin{aligned} E_1 &= E_1^0 + 2\omega_3(C_3 + C_6(\mu_{12}^0)^2 - C_{12}\mu_{12}^0) \\ E_2 &= E_2^0 + 2\omega_3(C_6 + C_3(\mu_{21}^0)^2 - C_{12}\mu_{21}^0) \\ \mu_{12} &= \mu_{12}^0 + \omega_3 \tfrac{1-\mu_{12}^0\mu_{21}^0}{E_2^0}(C_{12} - 2C_6\mu_{12}^0) \\ \mu_{21} &= \tfrac{E_2}{E_1}\mu_{12};\ \mu_{12} \gg \mu_{21} \\ G_{12} &= \tfrac{E_2}{2(1+\mu_{12})}, G_{23} = G_{13} = G_{12} \end{aligned}\right\} \quad (6)$$

where E_1, E_2, μ_{12}, μ_{21} and G_{12} are the elastic moduli, Poisson's ratios and shear modulus of the thin wall composite shell with crack damage, respectively. E_1^0, E_2^0, μ_{12}^0, μ_{12}^0 and G_{12}^0 are their counterparts in the intact composite structure, respectively. C_1–C_{12} are material coefficients independent of strains and damage, but dependent on the composite configuration, i.e., fiber geometry and orientations, fiber volume fraction, ply stacking sequence, etc. These parameters can be determined by measuring the specimen made of the same composite materials. Let ω_3 be a variable representing the crack damage status, which is related to the number, length and width of the crack. It can be expressed as

$$\omega_3 = \eta_c \bar{a}_c \bar{b}_c \bar{f}_c \quad (7)$$

where η_c is the crack density, which is defined as the crack number in a unit area; $\bar{a}_c$ and $\bar{b}_c$ are the average length and width of the crack, respectively, and $\bar{f}_c$ is an adjustment coefficient, which has been discussed in ref [26].

For other types of damage in a resin glass fibre structure, such as delamination, the variations of local elastic modulus can also be calculated using Eq. (6) with its corresponding material coefficients.

3. Experimental verification of FE model using measured FRF

The FE model is used to generate the training samples for ANN. Although it is impossible to have the FE model completely matched with the experiment specimen, high accuracy is still necessary in order to show the tendency of change in structural dynamic characteristics due to damages. It is understandable that, if the difference in dynamic characteristics between the FE simulation and the experiment data are large, the trained ANN using the FE model will definitely fail to identify the damage status of the experiment specimen. Therefore, the accuracy of the FE model should be verified first.

The FRF's of an empty laminated composite shell and a LCSFF are calculated and compared with experimentally measured results. In addition to verification of the FE model, this experiment can also help to determinate the sensors' locations, which will be discussed in Section 5.

During the experiment, the LCSFF specimen was put on a large piece of soft sponge to achieve free boundary conditions. The structure was excited by a B&K 8206 impact hammer at location 1 and the responses were measured at location 2 (see Fig. 1) by B&K 4397 piezoelectric deltaShear accelerometers connected to a B&K 2635 Charge amplifier (see Fig. 2). The FRF was measured using a Brüel & Kjær (B&K) 2035 Signal Analyzer unit.

The measured and computed magnitudes of the FRF for the empty shell and shell partially filled with water ($H/L = 0.7826$, H: height of fluid's surface lever; L: length of the shell) are shown in Figs. 3 and 4, respectively.

Natural frequencies can be obtained from FRF data. The measured and computed natural frequencies for the empty shell and the LCSFF are tabulated in Tables 1 and 2, respectively. The modes of vibration are denoted by a circumferential nodal number n and the axial nodal number m throughout the paper. Because the LCSFF studied in this paper is an axially symmetric structure, all natural frequencies listed in Tables 1 and 2 are in fact repeated natural frequencies. Table 1 shows a maximum error of 1.295% for the first two natural frequencies of the empty composite shell. Table 2 shows that the maximum error is 3.765% and the average error is 2.152% for the first seven natural frequencies of the LCSFF with water level $H/L = 0.7826$. The agreement between numerical and experimental results is generally satisfactory.

There are some modes in which only the fluid part is deformed while the shell part is kept undeformed. Therefore, these modes cannot be measured by the sensors attached on the side wall of the LCSFF. Besides these fluid modes, the numerically calculated mode with a natural frequency of 1349.7 Hz has no corresponding measured data, because this mode is mainly due to the deformation of the bottom of the LCSFF. There is no discriminable peak for this mode even in the computed FRF curve shown in Fig. 4.

It can be seen from Figs. 3 and 4 that the numerically simulated and measured FRFs are very similar, both for

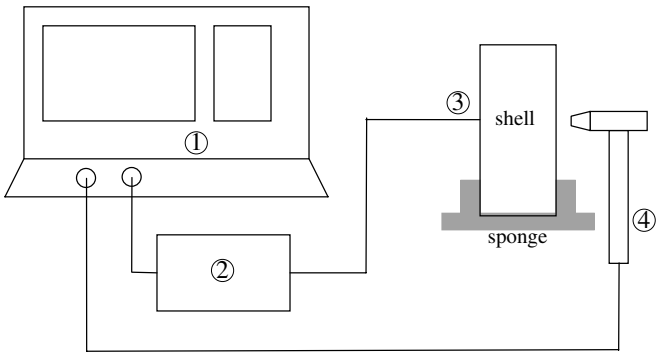

① Brüel & Kjær (B&K) 2035 Signal Analyzer Unit
② B&K 2635Charge Amplifier
③ B&K 4397 piezoelectric deltaShear accelerometers
④ B&K 8206 impact hammer

Fig. 2. Schematic diagram of experimental set-up for a FRF measurement.

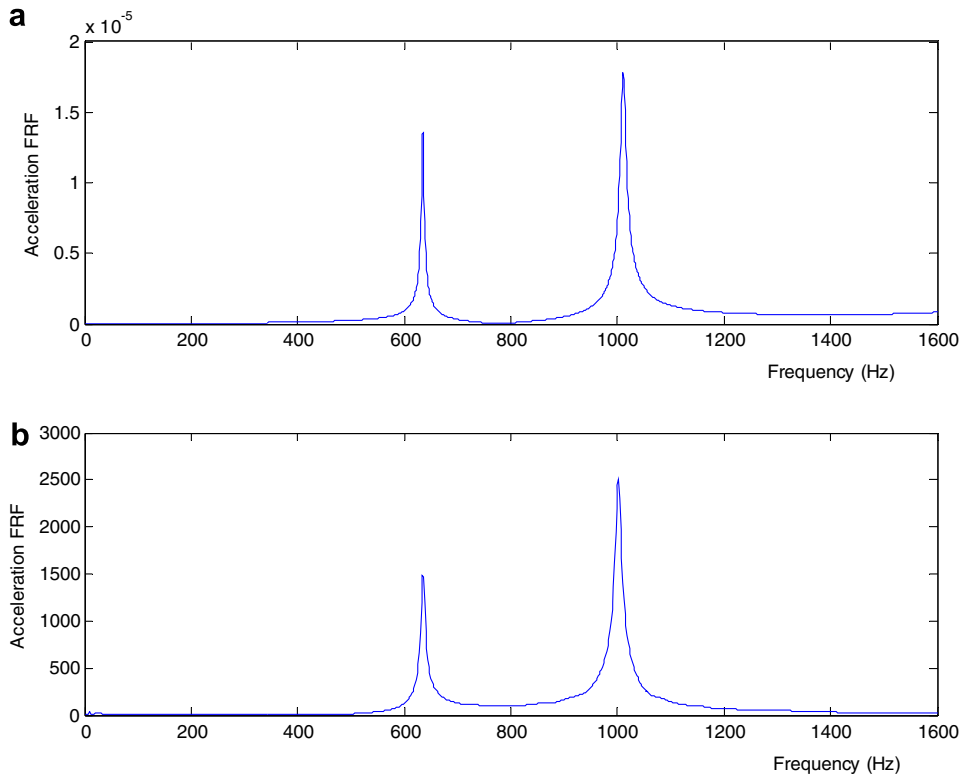

Fig. 3. Measured and computed FRFs of the empty shell: (a) calculated; (b) measured.

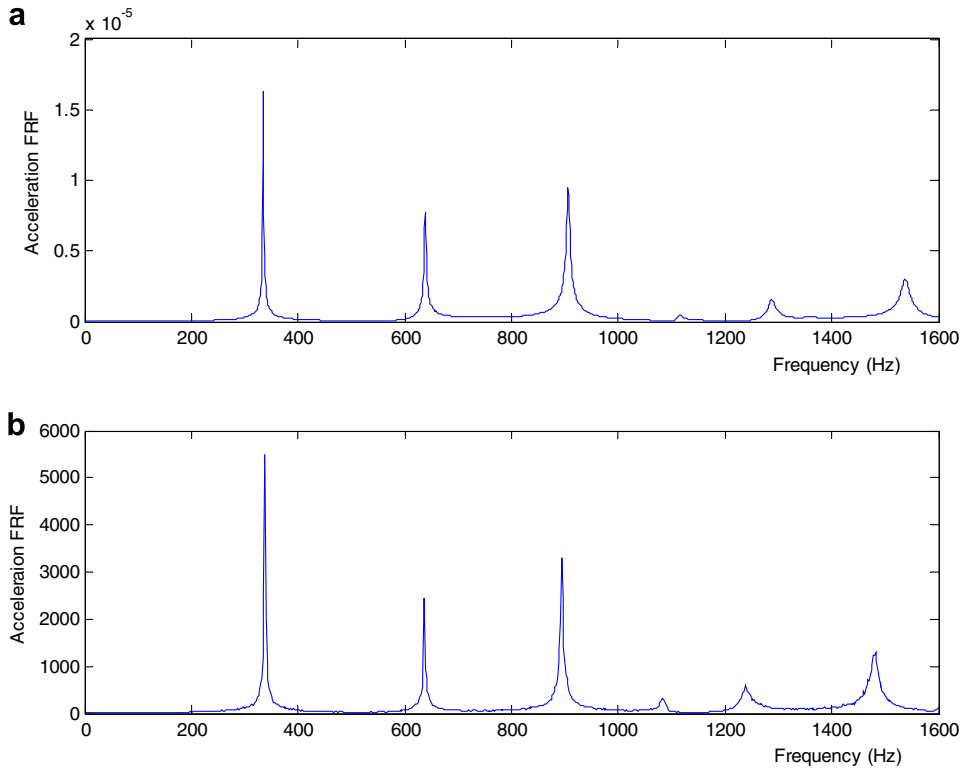

Fig. 4. Measured and computed FRFs of the static LCSFF with $H/L = 0.7826$: (a) calculated; (b) measured.

the empty shell and the static LCSFF. It suggests that the FE model used in this paper can simulate the dynamic performance of the static LCSFF with satisfactory accuracy. A comparison between Figs. 3 and 4 clearly also shows a shift of the resonance peaks towards low frequency due to the mass loading of the fluid in LCSFF.

Table 1
Natural frequencies of the laminated composite cylindrical shell with $H/L = 0$

Mode		Experiment results (Hz)	FEM results (Hz)	Error (%)
m	n			
1	2	638	640.48	0.372
2	2	1006	1019.2	1.295

Table 2
Natural frequencies of the laminated composite cylindrical shell filled with water with $H/L = 0.7826$

Mode		Experiment results (Hz)	FEM results (Hz)	Error (%)
m	n			
1	2	338	336.08	0.568
2	2	636	639.21	0.505
2	3	894	906.34	1.380
3	3	1084	1115.9	2.943
3	2	1240	1286.5	3.750
1	1	–	1349.7	–
4	3	1482	1537.8	3.765
Average				2.152

4. Damage index

Changes in structural dynamic properties due to structural damage are generally very small. Yan and Yam [12] pointed out that when the crack length in a composite plate reached 1% of the plate length, the relative variation of the natural frequency is generally about 0.01–0.1%. For the static LCSFF studied in this paper, the relative variations of the natural frequency caused by two damages are tabulated in Table 3, respectively. The length of damage case 1 is 5 mm (1.785% of the model's height) and 10 mm (3.57% of the model's height) for case 2, both having the same width (1 mm), depth (0.5 mm) and location (shown in Fig. 1). All natural frequencies of the intact LCSFF listed in Table 3 are repeated natural frequencies. This is still the case for some modes after damage is introduced, while others are split into two close natural frequencies. It can also be seen that the sensitivities of natural frequencies to the damage are different. However, the relative variations of the natural frequency are generally less than 0.1%, and the absolute variations are all less than 1 Hz. This variation is too small to be observed in most of the experiments. Therefore, a more sensitive index needs to be found.

Due to the ability of performing local analysis on a signal, i.e. to zoom in any interval of time or space, wavelet analysis is capable of revealing some hidden aspects of the data that other signal analysis techniques fail to detect. Many works [11,25,27–30] have proved that the damage index built with wavelet analysis is sensitive to damage.

The wavelet transform of a continuous vibration response $x(t)$ is defined as

$$W_x(a,b) = (|a|)^{-\frac{1}{2}} \int_R x(t)\Psi^*\left(\frac{t-b}{a}\right) \mathrm{d}t \tag{8}$$

Table 3
Change caused by damage in natural frequencies of the LCSFF with $H/L = 0.7826$

Mode		Natural frequencies of intact LCSFF (Hz)	Natural frequencies of LCSFF with damage case 1 (Hz)	Percent of change (%)	Natural frequencies of LCSFF with damage case 2 (Hz)	Percent of change (%)
m	n					
1	2	336.08	336.02	0.0179	335.99	0.0268
2	2	639.21	638.92	0.0454	638.78	0.0673
2	3	906.34	905.95	0.0430	905.82	0.0574
			906.30	0.0044	906.00	0.0375
3	3	1115.9	1115.1	0.0717	1114.9	0.0896
			1115.9	0	1115.3	0.0538
3	2	1286.5	1286.4	0.0078	1286.2	0.0233
1	1	1349.7	1349.6	0.0074	1349.6	0.0074
			1349.7	0	1349.7	0
4	3	1537.8	1537.1	0.0455	1536.9	0.0585
			1537.7	0.0065	1537.2	0.0390

where b is the translation parameter; a the scale parameter; $x(t)$ the vibration response to be decomposed; $\Psi^*(t)$ the transforming function (mother wavelet); and W_x the calculated wavelet coefficients, which can be used to recompose the original function $x(t)$. The equation for recomposing $x(t)$ can be expressed as

$$x(t) = \frac{1}{C_\Psi} \int_{-\infty}^{+\infty} \int_{-\infty}^{+\infty} \frac{1}{a^2} W_x(a,b)\Psi\left(\frac{t-b}{a}\right) \mathrm{d}a\,\mathrm{d}b \tag{9}$$

where $C_\Psi = 2\pi \int_0^{+\infty} (|\Psi(r)|)^2 \,\mathrm{d}r/r$.

Various forms of wavelet base function $\Psi(t)$ have been developed.

One of wavelet methods introduced to damage detection is wavelet packet analysis (WPA) algorithm. WPA algorithm is a generalization of wavelet decomposition that offers a richer signal analysis. For a given orthogonal wavelet function, a library of wavelet packets bases is generated. Each of these bases offers a particular way of coding signals, preserving global energy and reconstructing exact features.

In the orthogonal wavelet decomposition procedure, the generic step splits the approximation coefficients into two parts. A vector of approximation coefficients and a vector of detail coefficients can be obtained after splitting, and both at a coarser scale. The information lost between two successive approximations is captured in the detail coefficients. The next step consists in splitting the new approximation coefficient vector; successive details are never reanalyzed.

In the corresponding wavelet packets situation, each detail coefficient vector is also decomposed into two parts using the same approach as in approximation vector splitting. This offers the richest analysis: the complete binary tree is produced in the one-dimensional case or a quaternary tree in the two-dimensional case. The algorithm used for the wavelet packets decomposition follows the same line as the wavelet decomposition process.

Details of WPA algorithm are discussed as follows:

Let $g_j^n(t) \in U_j^n$, then $g_j^n(t)$ can be expressed as

$$g_j^n(t) = \sum_l d_l^{j,n} u_n(2^j t - l) \tag{10}$$

In WPA decomposition algorithm, $\{d_l^{j,2n}\}$ and $\{d_l^{j,2n+1}\}$ can be calculated as follows:

$$\left.\begin{aligned} d_l^{j,2n} &= \sum_k a_{k-2l} d_k^{j+1,n} \\ d_l^{j,2n+1} &= \sum_k b_{k-2l} d_k^{j+1,n} \end{aligned}\right\} \tag{11}$$

and the formula for recomposing $\{d_l^{j+1,n}\}$ using $\{d_l^{j,2n}\}$ and $\{d_l^{j,2n+1}\}$ is

$$d_l^{j+1,n} = \sum_k [h_{l-2k} d_k^{j,2n} + g_{l-2k} d_k^{j,2n+1}] \tag{12}$$

The WPA method can adaptively choose the corresponding frequency bandwidth according to the characteristics of the signal to be analyzed, and the decomposed sub-wavelet functions possess orthogonality in both frequency and time domains.

Assuming that the original vibration response $x_{0,0}^{(i)}(t)$ at the ith measurement location of a structure is decomposed into $x_{L,j}^{(i)}(t)(j = 1, 2, \ldots, 2^{L-1})$, with L being the selected layer number of the wavelet tree, $x_{0,0}^{(i)}(t)$ can then be expressed as

$$x_{0,0}^{(i)}(t) = \sum_{j=1}^{2^{L-1}} x_{L,j}^{(i)}(t) \tag{13}$$

Let the energy of the jth order sub-signals of the intact and damaged structures be $U_{L,j}^0$ and $U_{L,j}^d$, respectively. A non-dimensional damage feature index vector can be composed as follows:

$$\begin{aligned} V_d &= \{v_1, v_2, \ldots, v_{2^{L-1}}\}^{\mathrm{T}} \\ &= \left\{1 - \frac{U_{L,1}^d}{U_{L,1}^0}, 1 - \frac{U_{L,2}^d}{U_{L,2}^0}, \ldots, 1 - \frac{U_{L,2^{L-1}}^d}{U_{L,2^{L-1}}^0}\right\}^{\mathrm{T}} \end{aligned} \tag{14}$$

After structural vibration response signals in time domain are decomposed into multiple sub-signals using wavelet transform, the change corresponding to structural damage in each subsignal may manifest notable difference, and some of the sub-signals may possess high sensitivity to small damage in structures. The energy of each sub-signal in a given time-interval is calculated in order to quantify variations in these sub-signals caused by structural damage, so that an energy spectrum can be formed for each structural vibration response. After damage, the energy spectrum is changed. The variation in energy spectrum of damage structure with respect to that of the intact structure is taken as the index of structural damage. In this paper, the WPA level is five, so the damage index has 32 elements; each of them corresponds to an energy spectrum of subsignals.

5. Measurement of response signals in experiment

5.1. Arrangements of actuator and sensors

The locations of actuators and sensors are determined based on the following considerations:

1. Symmetric character of the LCSFF.
   The LCSFF studied in this paper is axial symmetric. If the sensors are in the plan determined by the actuator and the axis of the LCSFF, the LCSFF model will be divided into two symmetric parts. Two damages with the same dimensions but at symmetric locations about this plan will have the same damage index. Then, the range of possibly damage location can be reduced by half. This will make remarkable timesaving in computing the train sample and the training process of the ANN.
   Using this method, the exact location of damage in one half of the model can be known. This however, cannot tell in which half the damage is. The two possible solutions can be referred as "true" and "ghost" solutions, respectively. However, determining the damage location from just two symmetric candidate locations is very easy. As one of many possible methods, the identification after rotating the actuator and sensors around the axis of the LCSFF model needs to be repeated; and then combined results from these two-step identifications can finally give the exactly location of the damage. Although one additional time of measurement and ANN identification are needed, it is still worthy to adopt this two-step identification method.
2. Rigid body motion in measured signals.
   Same as the FRF experiment, the LCSFF specimen is put on a large piece of sponge to realize the free boundary conditions, which will lead to the problem of rigid body motion. The rigid body motion is however excluded in the computation of response signals. In order to eliminate the rigid body motion from experiment, two axially symmetric sensors are needed. The rigid body motion can be eliminated by subtracting the response signals measured by sensor A from those measured by sensor B. Corresponding subtraction has also been conducted for the computed signals in order to be consistent with the measured signals. Furthermore, this subtraction can also eliminate some measurement noise, because these two signals are measured simultaneously and recorded by the same equipment.
3. Frequency components in the measured response signals.Because the structural damage information is distributed in different vibration modes, the measured response signals should contain as many frequency components as possible. The power spectral density (PSD) of the response signals is determined by the PSD of excitation signal and FRF of the model. In this paper, the adopted excitation signal is a 50 Hz square wave, which is suitable for vibration response based damage

detection as discussed in Ref [20]. Therefore, locations of actuator and sensors can be selected using its FRF as index.

After a simple search process based on the above consideration, the excitation force is selected at location 3 and two sensors are arranged at locations 2 and 4.

5.2. Measurement of the response signals in experiment and damage identification

A 50 Hz square wave is generated using a TGA 1241 arbitray waveform generator and amplified using a B&K 2706 power amplifier. It is then fed to the actuator, B&K 4890 Vibration Exciter, as the excitation signal. The output of the actuator is recorded after amplified using a B&K 2525 Measuring Amplifier. The response signals are measured by two B&K 4397 piezoelectric deltaShear accelerometers connected to a B&K 2635 charge amplifier. A B&K 2035 signal analyzer unit is used to record the actuate and response signals (see Fig. 5).

Using piezoelectric accelerometers and vibration exciter instead of embedded and/or surface mounted piezoceramic patches will not affect the effectiveness of the present method for online damage detection, since the types of the sensors and actuators are not the kernel of the present method. If this method were proved feasible when using piezoelectric accelerometers and vibration exciter, it would be reasonable to believe that this method can work well when using embedded and/or surface mounted piezoceramic patches.

In order to eliminate the noise, the measurement of response signals is conducted in the following two steps. Firstly, the measurement begins when the experiment specimen has been excited for a while and the response signals are steady. Secondly, the measurement repeats five times. Then the averages of these five measurements are computed as the final results.

6. Damage identification by ANN

After establishing the FE model of intact and damaged static LCSFF, damage indices of a static LCSFF with various damage locations and lengths can be simulated, and then an ANN can be trained using the simulated data, and then adopted to identify the practical structural damage.

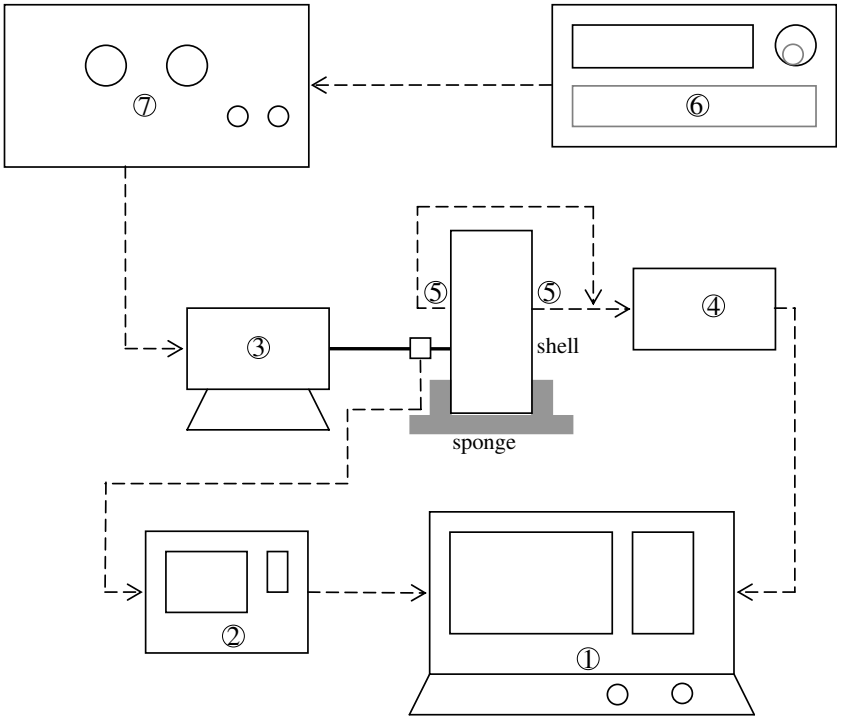

① Brüel & Kjær (B&K) 2035 Signal Analyzer Unit
② B&K 2525 Measuring Amplifier
③ B&K 4890 Vibration Exciter
④ B&K 2635Charge Amplifier
⑤ B&K 4397 piezoelectric deltaShear accelerometers
⑥ B&K 2706 Power Amplifier
⑦ TGA 1241 Arbirtray Waveform Generator

Fig. 5. Schematic diagram of the experimental set-up for response measurement.

6.1. Design of ANN

Experience accumulated from exploratory investigations is still the main guideline for design of ANN, because there appears to be a lack of a generic procedure in the design of ANN according to the character of the identification problem itself.

Among many different forms of network topologies, the multi-layer feed-forward (MLP) network, which possesses layered structure and allows only connections from neurons in one layer to those in the forward layers, has been widely applied due to its effectiveness and simplicity. A typical MLP network mainly includes the input layer for receiving input data, the hidden layer for processing data and the output layer to indicate the identified results.

The design of an MLP includes the selection the numbers of neurons in the input, hidden and output layers, the number of hidden layers and transfer function for each layer.

The numbers of neurons in the input and output layers are determined by damage index (input data) and damage status code (output data). The present damage index has 32 elements. Then, the input layer has 32 neurons. Because the mesh in present FE model is regular, the damage status can be expressed by three numbers: the row and column number of the damaged element, and the length of the crack. The row number is counted from the bottom to the top of the model. The column number is counted clockwise and the column at the right of sensor A is selected as the first column. Then the output layer has 3 neurons.

It has been proven that a network with only one hidden layer can approximate any continuous function to arbitrary accuracy if the number of hidden neurons H is sufficiently large [31,32]. Moreover, most of the work in damage detection adopted MLP with only one hidden layer. Therefore, one hidden layer is adopted.

H should be chosen according to the complexity of the problem processed by the network. If the H, is too small, the capability of the network will be restrained. Eberhart R.C. and Dobbins R.W. suggested that H should not be less than $\sqrt{N+o}$, where N and o are the neuron numbers of input layer and output layer, respectively [33]. Zang and Imregun suggested that H should be selected as half of N [34]. In the present case, N has been determined as 32, and o is 3. Then, H is selected as 16, which is half of N and is larger than $\sqrt{N+o} = \sqrt{35}$.

Same as most of the MLP neural networks, the transfer function of the hidden layer and output layer is selected as Tan-Sigmoid transfer function and Liner transfer function, respectively.

6.2. Training of the ANN

The training process of an MLP neural network includes providing training data (data patterns) to the MLP neural network and adjusting the interconnection weights continuously according to the error of outputs until a predefined error criterion is reached.

Before the damage index and damage status code are directly used in the training procedure, a data scaling process is usually required. The damage index and damage status code are normalized to fall within a prescribed region. The values of the present damage index are limited by its nature, so it does not need to be normalized. The code of damage status is normalized as follows: the row and column number are normalized by dividing them by the total row number and the total column number, respectively; the lengths of the cracks are expressed as

$$C = \frac{L_c}{L} \cdot 10 \tag{15}$$

where C is the coding value of the lengths of cracks, L_c the actual lengths of cracks, and L the height of the LCSFF. The maximal length of crack studied in this paper is 10% of L, so the value of C calculated from Eq. (15) will be in the range of [0 1].

The determination of the training sample number and the training precision of the ANN is an ongoing topic. Hasselman and Anderson [35] suggested a design criterion $s = 1 + H(N + o + 1)/o$ for the number of training samples, where s is the number of training samples. According this criterion, the vibration responses of 192 damaged cases and one intact case are numerically simulated using FEM. The damage length of these 192 samples is randomly selected and ranges from 2% to 10% of the height of the LCSFF; all damages are evenly distribute in one half of the shell. Then, damage indices of these 192 damage cases are obtained by comparing the energy spectrum of the decomposed wavelet signals for each case with that of the intact structure. Then, the widely used Levenburg–Marquardt back-propagation training algorithm is adopted to carry out the neural network learning towards minimizing a predefined error function, which is generally formulated as the mean square error between the network outputs and the actual values corresponding to the given set of input vectors. As a result, an optimal set of weights are obtained.

6.3. Identification of the damage status by numerical simulation

Damage indices of two other damage cases are numerically simulated. These two damage cases, case A and case B, are taken as verification samples after the training process. The damage length in case A and case B are 4% and 5%, respectively. Their locations are shown in Fig. 1.

Feeding the damage index of case A to the ANN yields the following result: (0.4923, 0.9390, 0.9195). These three numbers means the scaled length, scaled column and row numbers. The corresponding physical values are (4.923, 11.268, 11.034). It means that the damage length is 4.923% of L (the height of the LCSFF), and the column and row numbers of the damaged element are both equal to 11 (The column and row numbers are rounded to integer.). Because of symmetry, the damage may also be located at (14, 11) element. Determining the final damage

Table 4
ANN identification results of case A and case B

	Results of the ANN identification	Converted result	Real damage status
Case A	(4.923, 11.266, 11.034)	(4.923, 11, 11) (4.923, 14, 11)[a]	(5, 14, 11)
Case B	(3.978, 2.982, 8.883)	(3.978, 3, 9) (3.978, 22, 9)[a]	(4, 3, 9)

[a] Ghost solution.

location from the above two symmetric candidate locations is easy in both theory and experiment, and can be realized using the present method. Therefore, this part is neglected. If the real damage location is included in the two symmetric candidate locations, the target of validating the present method is achieved.

The converted results for case A and case B are tabulated in Table 4. Compared with the real damage status, the ANN obviously provides satisfactory accuracy in damage identification for the LCSFF.

6.4. Identification of damage status by experiments

In the test specimen, a crack is machined using a 75-watt Epilog's Legend 36EXT laser engraving and cutting system that has 1200 DPI engraving resolution. The dimensions of the damage are 10 mm in length (3.57% of the LCSFF's height), 1 mm in width and 0.5 mm in depth (see Fig. 6).

The damage index acquired from the experimentally measured data and the numerically simulated data are shown in Fig. 7. Despite local difference in the simulated damage index and the measured one, the relative magnitudes between the elements for these two sets of data are similar. Taking the measured damage index as the input

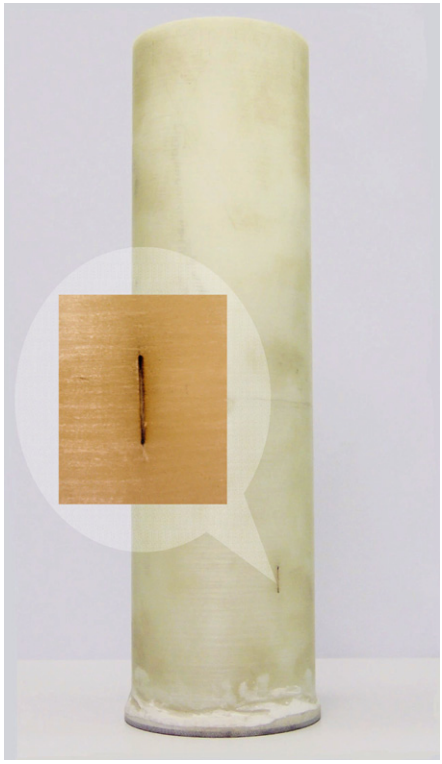

Fig. 6. Damage case in the test specimen.

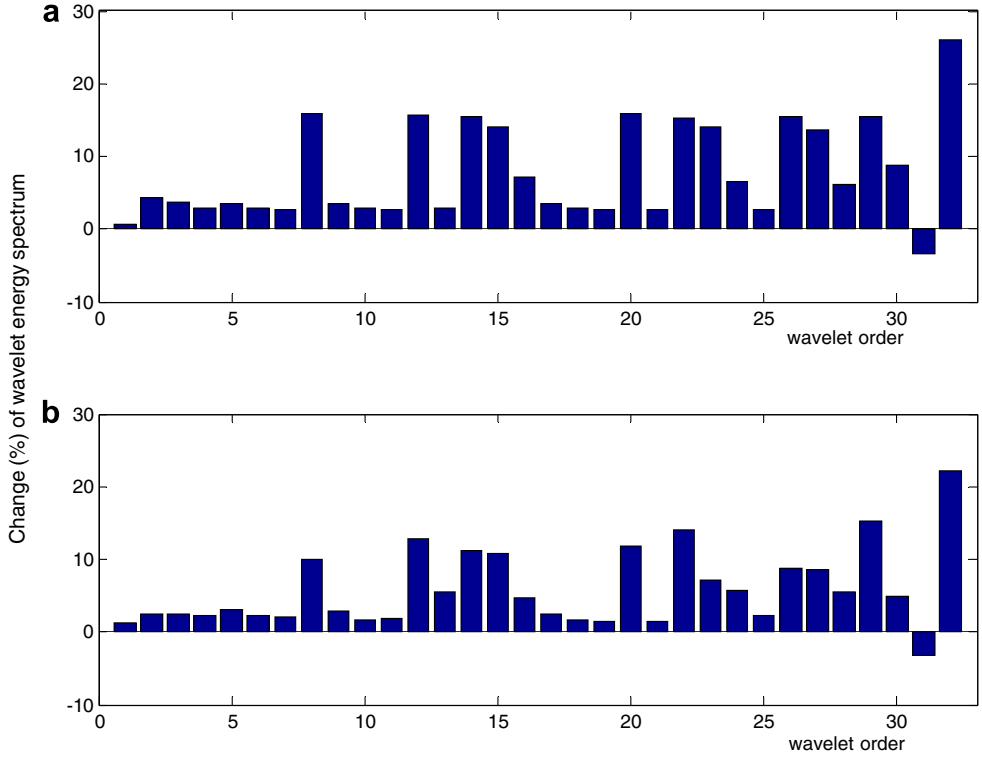

Fig. 7. The measured and computed damage indices: (a) calculated; (b) measured.

of the trained ANN, the converted results are (3.1, 4.109, 4.934). The identified length of damage is 3.1% of the LCSFF height, which is a slightly smaller than the true vale: 3.57%. The second and the third number, once rounded to integer numbers, give the right location of the damage: (4, 5). The error is due to the unavoidable difference between the simulated damage and the actual structural damage, and the effect of the exciter attachment. Generally speaking, the presented damage detection method for the static LCSFF is shown to provide a reliable result when compared with the reality.

7. Conclusions

In this paper, the damage detection for a static LCSFF is studied with numerical simulation and experimental validation. The following conclusions can be drawn:

1. The change in natural frequencies of the LCSFF due to the small damage is generally very small. For instance, this change is less than 0.1% when the damage length is 1% of the structural height. Therefore, the change in natural frequencies is not a suitable damage index for the static LCSFF.
2. The change in energy spectrum of the decomposed wavelet signals of structural dynamic responses provides a more sensitive damage index. Then conventional ones, suitable to be used in LCSFF structure.
3. A MLP neural network trained using the numerically simulated data can successfully identify the damage status of the static LCSFF.

Experimental results validated the method presented in this paper. The overall methodology proposed in this paper provides a practical and relatively reliable tool for the damage detection of the LCSFF.

Acknowledgements

The authors thank for the support by the Research Grants Council of Hong Kong Special Administrative Region of China under the Project No. PolyU 5313/03E; and Natural Science Foundation of China under the Grant 50375123. The second author wishes to acknowledge the support from a special fund for new Chair Professors given by The Hong Kong Polytechnic University.

References

[1] Schultz AB, Warwick DN. Vibration response: a nondestructive test for fatigue crack damage in filament-reinforced composites. J Compos Mater 1971;5:394–404.
[2] DiBennedetto AT, Gauchel JV, Thomas RL, Barlow JW. Nondestructive determination of fatigue crack damage in composites using vibration tests. J mater 1972;7:211–5.
[3] Banks HT, Inman DJ, Leo DJ, Wang Y. An experimentally validated damage detection theory in smart structures. J Sound Vib 1996;191:859–80.
[4] Tseng KK, Naidu ASK. Non-parametric damage detection and characterization using smart piezoceramic material. Smart Mater Struct 2002;11:317–29.
[5] Staszewski WJ, Pierce SG, Worden K, Philp WR, Tomlinson GR, Culshaw BR. Wavelet signal processing for enhanced Lamb wave defect detection in composite plates using optical fibre detection. Opt Eng 1997;36:1877–88.
[6] Vestroni F, Capecchi D. Damage detection in beam structures based on frequency measurements. J Eng Mech 2000;126:761–8.
[7] Worden K. Structural damage detection using a novelty measure. J Sound Vib 1997;201:85–101.
[8] Hwang HY, Kim C. Damage detection in structures using a few frequency response measurements. J Sound Vib 2004;270:1–14.
[9] Duan ZD, Yan GR, Ou JP, Spencer BF. Damage localization in ambient vibration by constructing proportional flexibility matrix. J Sound Vib 2005;284:455–66.
[10] Au FTK, Cheng YS, Tham LG, Bai ZZ. Structural damage detection based on a micro-genetic algorithm using incomplete and noisy modal test data. J Sound Vib 2003;259(5):1081–94.
[11] Chen Q, Chan YW, Worden K. Structural fault diagnosis and isolation using neuralnetworks based on response-only data. Comput Struct 2003;81:2165–72.
[12] Yan YJ, Yam LH. Online detection of crack damage in composite plates using embedded piezoelectric actuators/sensors and wavelet analysis. Compos Struct 2002;58:29–38.
[13] Kullaa J. Structural health monitoring under variable environmental or operational conditions. In: Proceedings of the second european workshop on structural health monitoring, M[udblac]nchen, Germany; 2004. p. 1262–9.
[14] Wordeny K, Sohn H, Farrar CR. Novelty detection in a changing environment: regression and interpolation approaches. J Sound Vib 2002;258(4):791–9.
[15] Roberts S, Tarassenko L. A probabilistic resource allocating network for novelty detection. Neural Comput 1994;6:270–84.
[16] Kao CY, Hung SL. Detection of structural damage via free vibration responses generated by approximating artificial neural networks. Comput Struct 2003;81:2631–44.
[17] Chou JH, Jamshid G. Genetic Algorithm in structural damage detection. Comput Struct 2001;79:1335–53.
[18] Pawar PM, Ganguli R. Genetic fuzzy system for damage detection in beams and helicopter rotor blades. Comput Meth Appl Mech Eng 2003;192(16–18):2031–57.
[19] Worden K, Manson G. Experimental validation of a structural health monitoring methodology: part I. novelty detection on a laboratory structure. J Sound Vib 2003;259(2):323–43.
[20] Yam LH, Yan YJ, Jiang JS. Vibration-based damage detection for composite structures using wavelet transform and neural network identification. Comput Struct 2003;60:403–12.
[21] Fenves SJ. Numerical and computer methods in structural mechanics. New York: Academic Press; 1973.
[22] Taylor RL, Beresford PJ, Wilson EL. A non-conforming element for stress analysis. Int J Numer Meth Eng 1976;10:1211–9.
[23] Mazúch T. Determining the acoustic natural modes and frequencies of irregular shaped rigid walled cavities by FEM. J Czech Slovak Mech Eng 1993;44:433–40.
[24] Yan YJ, Yam LH, Cheng L, Yu L. FEM modeling method of damage structures for structural amage detection. Comput Struct 2006;72:193–9.
[25] Ovanesova AV, Suárez LE. Applications of wavelet transforms to damage detection in frame structures. Eng Struct 2004;26:39–49.
[26] Talreja R. Damage mechanics of composite materials. Composite materials series, vol. 9. Amsterdam: Elsevier; 1994.
[27] Li B, Chen XF, Ma JX, He ZJ. Detection of crack location and size in structures using wavelet finite element methods. J Sound Vib 2005;285:767–82.
[28] Hou Z, Noori M, Amand RSt. Wavelet-based approach for structural damage detection. J Eng Mech ASCE 2000;126:677–83.

[29] Wang Q, Deng XM. Damage detection with spatial wavelets. Int J Solids Struct 1999;36(23):3443–68.
[30] Staszewski WJ. Wavelet based compression and feature selection for vibration analysis. J Sound Vib 1998;211(5):735–60.
[31] Funahashi KI. On the approximate realization of continuous mappings by neural networks. Neural Netw 1989;2(3):183–92.
[32] Hecht-Nielsen R. Counter-propagation networks. In: Proceedings of the international conference on neural networks; 1987. p. 19–32.
[33] Eberhart RC, Dobbins RW. Neural network PC tools: a practical guide. New York: Academic Press, Inc.; 1990.
[34] Zang C, Imregun M. Structural damage detection using artificial neural networks and measured FRF data reduced via principal component protection. J Sound Vib 2001;242:813–27.
[35] Hasselman TK, Anderson MC. Linking FEA and SEA by principal components analysis. In: Proceedings of the 16th international modal analysis conference, Santa Barbara, CA; 1998. p. 1285–91.